

$J_c - B$ performance study of an OCMG (Nd–Eu–Gd)-123 material doped by sub-micrometre Gd-211 particles

M Jirsa¹, M Muralidhar², M Murakami², K Noto³, T Nishizaki⁴
and N Kobayashi⁴

¹ Institute of Physics, ASCR, CZ-182 21 Praha 8, Czech Republic

² ISTEC/SRL, Division 3, 1-16-25 Shibaura, Minato-ku, Tokyo 105, Japan

³ Iwate University, Faculty of Engineering, 4-3-5 Ueda, Morioka, Iwate 020-08551, Japan

⁴ Institute for Material Research, Tohoku University, Sendai 980-77, Japan

Received 10 October 2000

Abstract

A concentration profile of Gd₂BaCuO₅ (Gd-211) fine particles embedded in an oxygen-controlled melt-grown (Nd_{0.33}Eu_{0.33}Gd_{0.33})Ba₂Cu₃O_{7-y} (NEG-123) material is studied. The secondary phase had a nominal content of 30 mol% and was refined by the addition of 0.5 mol% Pt and 1 mol% CeO₂. The main concern of this paper is devoted to the variation of the magnetic properties and Gd-211 phase distribution in a bulk NEG-123 pellet of 1.8 cm in diameter and 1 cm in height. $J_c(B)$ dependences deduced from magnetic hysteresis curves measured by SQUID were analysed with respect to the appearance of the central and second peaks. A successful fit of all the curves by an analytical function composed of two additive contributions representing the central and second peaks is reported. The separation of these two contributions revealed that the shape of the high-field part of the magnetization curves is mostly governed by the pinning mechanism(s) responsible for the second peak and no 'background' from another source of pinning is involved.

1. Introduction

The peak- or fishtail effect in RE-123 materials is of a paramount importance for bulk high T_c superconductor (HTSC) applications. The character of pinning sites producing a peak effect has been identified as a random point-like pinning disorder [1, 2]. What kind of the pinning defect prevails in the particular superconducting system and what is the underlying vortex dynamics, are still matters of vivid discussions. Oxygen deficiency is often declared as a principal source of this kind of pinning in RE-123 materials [1, 3, 4]. Some studies show a primary role of RE–Ba substitution in RE-123 materials with RE = Sm, Nd, Eu, or Gd [5, 6], the effect of this substitution being ascribed either to core pinning [7, 8] or to magnetic scattering [9]. In addition, fine secondary-phase particles have been also shown to enhance the second peak [10, 11]. To be able to identify individual contributions, rich experimental material needs to be collected. In the present work we report on the study of a series of samples taken from different places of one NEG-123 pellet doped with 30 mol% of fine Gd-211 particles. As all the samples were prepared

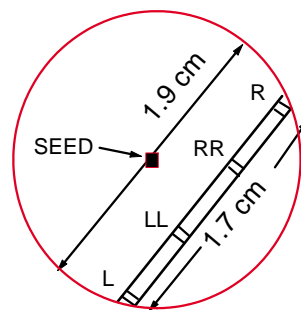


Figure 1. Schematic view of the samples displacement in the original pellet of a melt-textured NEG-123 material.

under same conditions, they differ only statistically in the distribution of the secondary-phase particles and in fluctuation of the matrix properties. We try to explore the fact that these two kinds of potential pinning defects are of significantly different sizes and to correlate their effect to different parts of the magnetization hysteresis loop and associated critical currents.

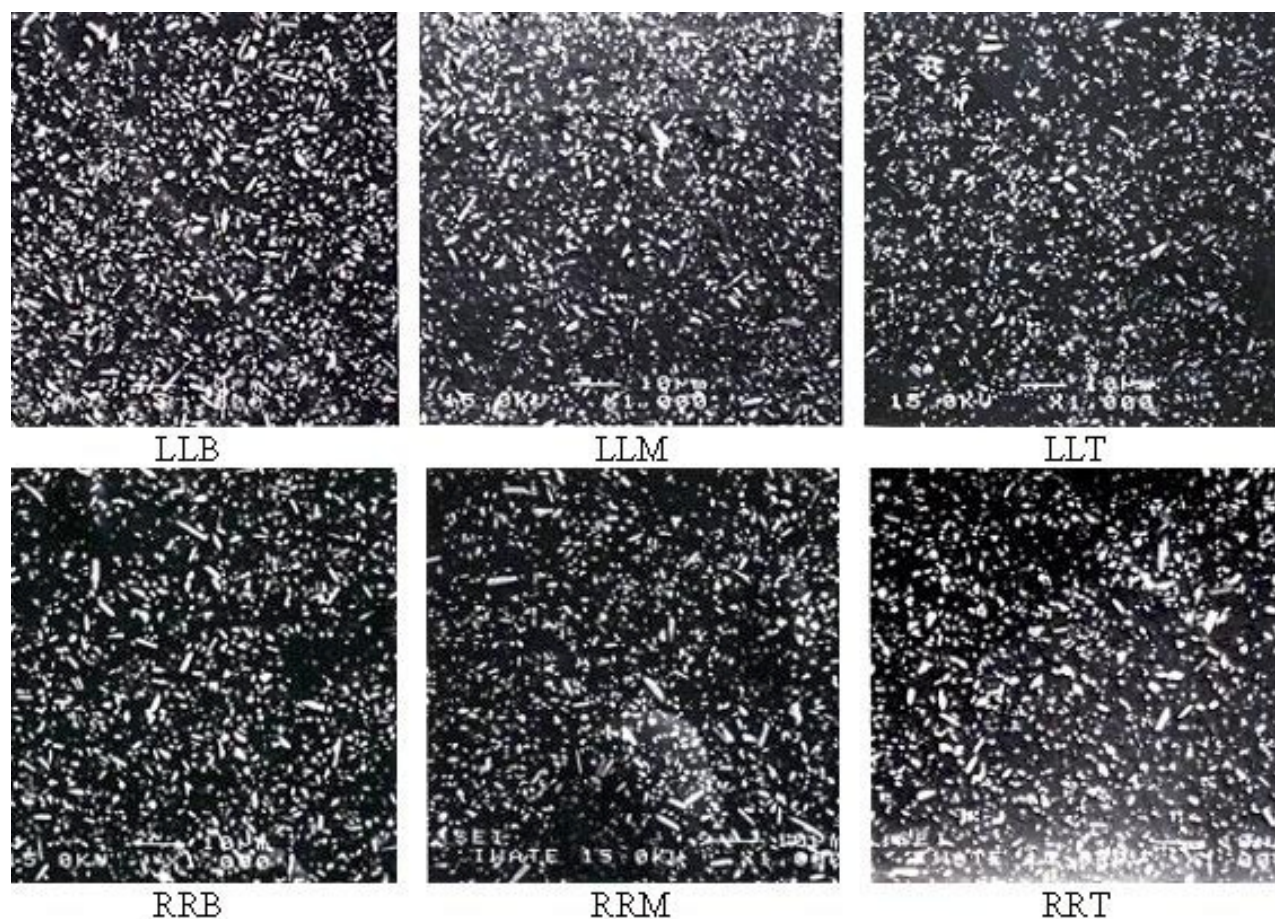


Figure 2. SEM images of the samples LL (upper row) and RR (lower row). The morphologies of samples L and R are very similar.

2. Experimental details

We studied oxygen-controlled-melt-growth processed NEG-123 samples with 30 mol% of Gd-211 particles refined by the addition of 0.5 mol% Pt and 1 mol% CeO₂. The exact technological treatment is described in [12]. A slice 1.5 mm thick was cut from the pellets 18 mm in diameter and 10 mm in height, 3.5 mm from the seed (see figure 1). From the slice, four vertical bars were cut, denoted L, LL, RR, and R, as indicated in the figure. From each bar, three samples were finally prepared, cut from the top, middle, and bottom of each bar. All 12 samples were annealed together in a 1 bar O₂ atmosphere at 600 °C to 300 °C for 240 h. After polishing the samples, magnetic hysteresis curves at 77 K were measured by a commercial 7 T QuantumDesign SQUID, with the field aligned along the *c*-axes. Critical current densities were calculated from magnetic hysteresis curves using the extended Bean model for a thin prism magnetized along the normal to the plane. The sample morphology was investigated by scanning electron microscopy (SEM) with the aim to check variation in the Gd-211 particles distribution within the pellet. The quality of the samples was checked by measuring the dc susceptibility as a function of temperature, both in the zero-field-cooled and field-cooled regimes.

3. Results and discussion

3.1. Local variation of 123-matrix properties

All 12 samples investigated showed practically the same concentration and average size of the Gd-211 particles (see figure 2). The average size of the particles was below 1 μm, the smallest particles being of about 0.1 μm in diameter. This proved that the technological process is able to produce samples with a homogeneous distribution of fine secondary-phase particles embedded in the RE-123 matrix. As has recently been shown, secondary-phase particles are effective in enhancing remanent critical currents [11, 12] (size of the central peak in the magnetic hysteresis loop (MHL)). The homogeneous distribution of fine secondary-phase particles in our samples also reflected in only weakly varying height of the central peak in the 12 samples. In all the samples, MHLs were measured up to 7 T and the critical currents calculated for the central peak maximum reached, at $T = 77$ K, values around $70 \text{ kA cm}^{-2} \pm 10\%$. The irreversibility field was typically around 6 T and, also, varied only little. The secondary peak was present in all the samples and lay at fields of 1.7–1.8 T, but its height strongly varied from sample to sample. Figures 3(a)–3(d) show the $J_c(B)$ curves of the samples L, R, LL, and RR, respectively. In the bars L and R the $J_c(B)$ dependence exhibited the best developed second peaks for the top samples, in the middle samples the

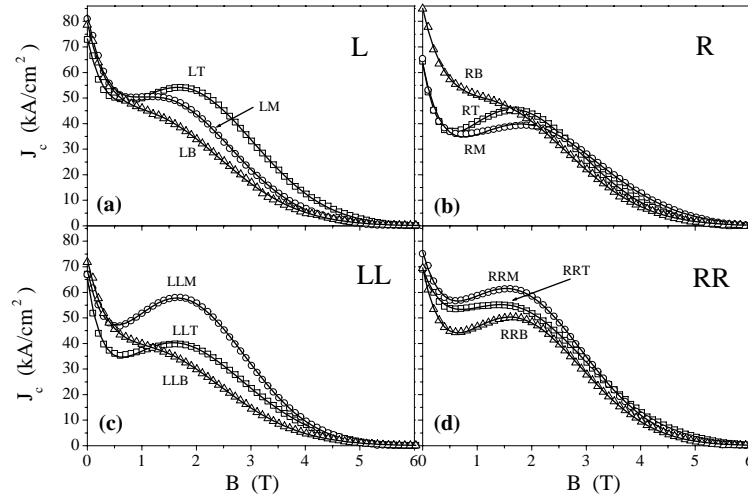


Figure 3. $J_c(B)$ curves measured by a SQUID magnetometer at 77 K for the (a) L, (b) R, (c) LL, and (d) RR samples. The three curves in each figure correspond to the top (T), middle (M), and bottom (B) sample of the given bar as denoted in the figures. The full curves are fits by means of equation (4).

second peaks were intermediate and in the bottom samples the second peaks were strongly masked by the central peak (figures 3(a) and 3(b)). In the LL and RR bars the middle samples exhibited pronounced second peaks, the top samples had intermediate second peaks, and the weakest second peaks were again observed in the bottom samples (see figures 3(c) and 3(d)). The reason for the reduction of the second peak in the bottom samples can be probably associated with heavy sample contamination by ZrO_2 coming from the rods of the material used to support the NEG pellet during the melting process. As the melting temperature of Gd-211 particles is higher than that of the NEG-123 matrix, the second-phase particles stood nearly unaffected by the reaction with ZrO_2 . The contamination was proved by the temperature dependence of the dc susceptibility. While in the top and middle samples the superconducting transition started at around 93.6 K and was only 1–1.5 K wide, the curves of the contaminated samples were identical to other ones up to 80% of the superconducting transition, but then exhibited a long tail extending up to 85.5 K. Although these samples were evidently bad, they presented a good comparative material for considerations on the operative pinning in the studied material. Moreover, in one of these samples (RB) the central peak was so high that even with a poorly developed second peak the overall performance was comparable and at low fields even better than that of the RT and RM samples. As mentioned above, the distribution of the Gd-211 particles in the LLB sample was similar to that in the other samples.

Because of the ZrO_2 contamination of the pellet bottom the secondary peak was suppressed in the bottom samples, but all other features of the $J_c(B)$ curves were similar to those of the other samples. The fact that the rather strong variation of $J_c(B)$ at around the second peak position was not in correlation with changes in the morphology of the secondary phase leads us to the conclusion that the role of the Gd-211 particles in the formation of the second peak is indirect and only variation of the NEG-123 matrix properties on the microscopic scale is the principal source of pinning responsible for the fishtail

effect (FE) [13]. The way how the secondary phase particles can contribute to the second peak might be stacking faults in the 123-matrix that have been recently shown to appear in the vicinity of secondary-phase particles and are sufficiently small to act as point-like pinning centres [14].

Due to the equally good oxygenation of all the samples, as documented by the same high T_c values oxygen deficiency is considered to be of less importance for the observed variation in the 123-matrix properties. Both the Ba content fluctuation and the substitution of Ba by Nd, Eu, and Gd atoms suggests itself as an alternative source of the point-like pinning.

We also stress that the highest peaks in the R, RR, LL, and L positions were usually found in the top or middle samples, but no clear tendency was found to be able to conclude on the role of the growth rate during the melt texture process.

The present experiments provide further evidence that the fishtail (second) peak is strongly sensitive to the local fluctuation of the 123-matrix properties [13]. According to Lorentz microscopy studies [15], some evidently strong pinning centres in high- T_c materials cannot be identified with crystallographic defects in the 123-matrix even by high-resolution electron microscopy (HREM). The problem is complicated by the lack of a detailed understanding of the vortex-pin interaction mechanism.

3.2. Fit of $J_c(B)$ curves

Recently, the model of general thermally activated creep has been widely discussed [16–19]; this model elucidated the relationship between the static and dynamic approaches to the fishtail problem. On the basis of an analysis of experimental data in terms of this model, the pinning potential in a Tm-123 single crystal and, later, also in other RE-123 single crystals was identified as logarithmic. The commonly observed scalings of the $J_c(B)$ curves with temperature and electric field were shown to be associated with power-law field dependences of the characteristic parameters $J_0(B) \propto B^m$ and $U_0(B) \propto B^{-n}$ in the expression for the pinning

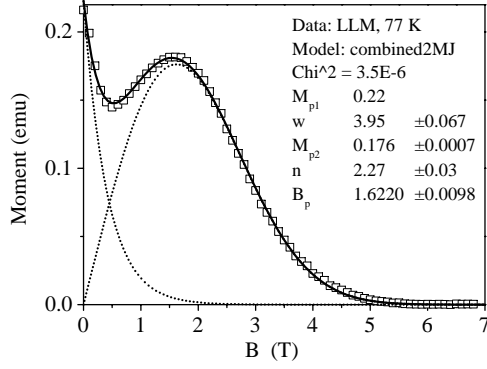


Figure 4. Fit of the experimental $J_c(B)$ curve measured in sample LLM at 77 K by means of equation (4). The broken curves are the separate contributions of the two terms in the equation, the full curve is their sum. We note the χ^2 value, indicating excellent quality of the fit.

energy $U(T, B, E, J) = U_0(T, B, E) \ln(J/J_0)$, with m and n positive. This model resulted in [16, 17]

$$J_c(B) \propto B^m \exp(cB^n). \quad (1)$$

The dependence (1) exhibits a maximum at $B = B_p$. From the condition for an extreme at $B = B_p, dJ_c/dB|_{B=B_p} = 0$, the constant c can be calculated, $c = -(m/n)B_p^{-n}$, which helps to transform relation (1) into [18]

$$J_c(B) = J_p b_p^m \exp[(1 - b_p^n)m/n] \quad (2)$$

with $J_p = J_c(B_p)$ and $b_p = B/B_p$.

In [18] we showed that in Dy-123 single crystal the central peak exhibits a different temperature scaling to the second peak. This indicates that the underlying pinning mechanisms are different. It was also shown that the field dependence of the central peak after the separation of the second peak is an exponentially decaying function,

$$J_c(B) \propto \exp(-wB). \quad (3)$$

A similar behaviour has been also observed in other RE-123 samples. Assuming that in the studied melt-textured samples the central peaks have similar characters, we combined the two contributions, (1) and (3), and obtained

$$J_c(B) = J_{p1} \exp(-wb_p) + J_{p2} b_p^m \exp[(1 - b_p^n)m/n] \quad (4)$$

where J_{p1} and J_{p2} denote the heights of the central and second peaks, respectively.

A special feature of relation (4) in the fits of experimental data of different RE-123 single crystals was that the parameter m could be set equal to one [16, 18, 20]. In the present work we also used this simplification. Thus, keeping $m \equiv 1$, we had four free parameters, w, n, J_{p2} , and B_p . J_{p1} was established from the experimental curves.

We note that the exponentially decaying functional dependence of the first term in (4) was found empirically in different samples, for example Dy-123 single crystals [18], Y-123 single crystal [21], La-systems [22], etc. In [23] such a field dependence was theoretically justified.

An example of a typical fitting procedure by means of equation (4) is the fit in figure 4 of the data measured on sample

LLM at 77 K. The broken curves are separate contributions of individual terms in equation (4), the full curve is their sum. The value of χ^2 shown in the figure implies the excellent fit quality.

In figures 3(a)–3(d) the full curves nearly coinciding with the experimental points represent the fits of the data by means of equation (4). In all cases the fit was nearly perfect.

We also fitted experimental data of two samples measured in a wide temperature range, namely sample LLM, with a very well developed second peak, and sample LLB, with the second peak rather depressed. The fits are presented as the full curves in figures 5 (sample LLM) and 6 (sample LLB). In all cases the fits were so good that it was difficult to distinguish them from the fitted experimental data; this applied to the whole investigated temperature range, 65–88 K. The fits enabled us to decompose the experimental curves into two additive contributions and study their temperature and field dependences separately. This procedure showed that in a major part of the temperature range, the total $J_c(B)$ curve, in the fields above B_p is a maximum in practice due only to the contribution from the second term in equation (4). In other words, the first term (central peak) contribution to the total magnetic moment usually decays so rapidly that above B_p it becomes negligible.

The rather large (about 1 μm or slightly smaller) secondary-phase particles have been found to affect the central peak [11, 12]. Their presence has been also sometimes associated with an increase in the second peak [11, 12], but this effect was regarded as an increase of background on which the second peak sits [24, 25]. The present analysis brings evidence that the ‘background’ is limited to rather low fields, mostly below the maximum of the second peak. The potential effect of these particles most probably enters indirectly via some induced point-like defects such as stacking faults, stresses and tensions in the RE-123 matrix, etc that then contribute to the pinning mechanism responsible for the second peak. We believe that the relevant mechanism is core pinning. On the other hand, the pinning mechanism associated with secondary-phase particles seems to selectively contribute to the central peak only, being restricted to rather low fields. This might be surface pinning [26]. With increasing density of flux lines this type of pinning loses its efficiency. As the central peak was shown to reflect the geometry of the sample [27] and was identified with demagnetizing effects [27–29] or self-fields [16, 17], it is necessary to clarify how pinning on secondary-phase particles enhances the central peak.

In melt-textured materials with the addition of secondary-phase particles, the central peak decreases with increasing temperature more slowly than the second peak. This behaviour is opposite to that usually observed in single crystals with a well developed second peaks. The explanation might be just the specific type of pinning on secondary-phase particles. With increasing temperature the irreversibility field decreases and the field range is thus reduced to the range where the effectiveness of pinning on secondary-phase particles is higher. Therefore, the central peak becomes larger in comparison with the second peak and extends to higher fields with respect to B_p , even reaching B_{irr} . Nevertheless, at least a weak contribution of the second peak survives up to highest temperatures, thus giving an explanation for the rather peculiar shape of the MHL

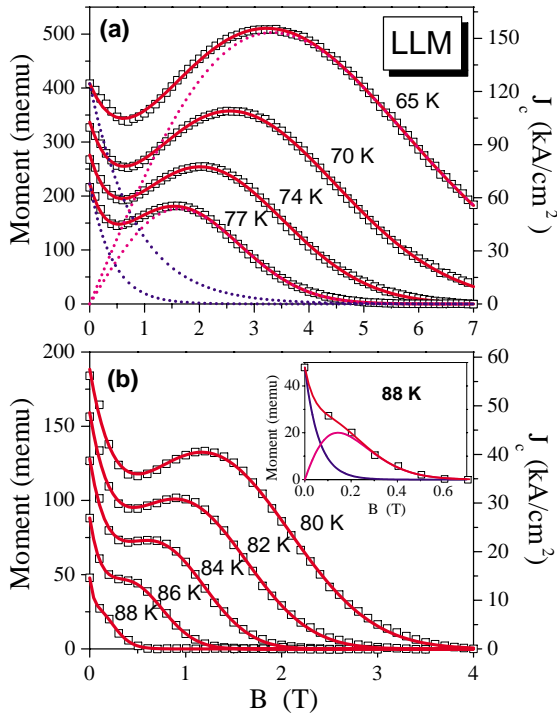


Figure 5. The upper parts of the MHL curves after correction for the paramagnetic contribution due to Nd, Eu and Gd ions and the associated critical current densities measured in sample LLM by means of SQUID magnetometry at temperatures (a) 65–77 K and (b) 80–88 K. The full curves are fits by equation (4), the broken curves indicate separate contributions of the central and second peaks. We note the existence of a significant J_c second peak even at 88 K (see the inset of (b)) where the total $J_c(B)$ curve does not explicitly show its presence.

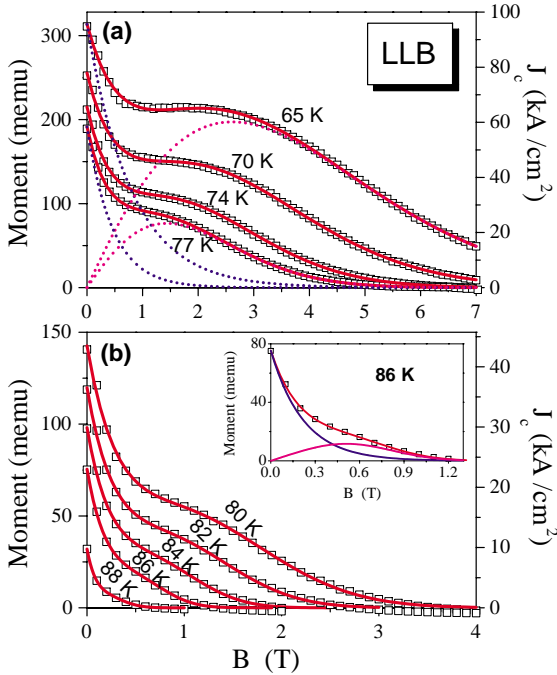


Figure 6. The same as in figure 5 but for the sample LLB and exhibiting a less pronounced second peak. Also, in this sample the second peak significantly participates to the total magnetic moment up to very high temperatures (see the inset of (b)).

at temperatures close to T_c . The increasing role of secondary-phase particles at high temperatures implies an enhancement of the specific volume pinning force of these particles with respect to point-like defects. This can be attributed to either a higher elementary pinning force density or a larger pinning volume. We believe that the latter case, which supports the idea of the surface pinning on secondary-phase particles, is more probable.

The excellent fit of the experimental data might be attributed to the relatively high number of free parameters involved; but for sample LLM with a well developed second peak (see figure 5), the position and height of the second peak on the experimental curve almost coincide with those of the separate theoretical curve (equation (2)). In this case we can fix B_p and J_{c2} at their experimental values and only two free parameters are left without any significant deterioration of the fit quality. In general, however, (e.g. sample LLB) we need all four free parameters. These four parameters allow us to fit the experimental curves of a large variety of shapes obtained at different temperatures.

At low temperatures the peak effect usually runs out of the accessible field range. In such a case only the low-field one part of the peak is available. Once we had determined the fit parameters from the low-field part, we could predict the course of $J_c(B)$ even beyond the experimentally accessible field range and estimate the value of B_{irr} . It is interesting to note that the $J_c(B)$ dependence in vicinity of B_{irr} is in most of the experimental range governed only by the second term in (4). The extrapolated B_{irr} value is therefore given not only by the fitting parameters themselves, but also by a precision criterion or resolution connected with J_c estimation.

The separation of the two pinning mechanisms revealed that the high-field slope of the second peak is governed mainly by pinning on a point-like disorder. This behaviour was observed in all temperatures below 86 K. Independent support for this conclusion follows from the pinning force density scaling as discussed below.

Temperature dependences of the fitting parameters of samples LLM and LLB are shown in figures 7(a)–7(c). The exponential decay rates w and n of both samples are nearly constant in the temperature range 65–77 K (figure 7(a)). This result was confirmed both by SQUID and vibrating sample magnetometry (VSM) measurements. Note that the temperature independence of the parameter n is an indication that the experimental $J_c(B)$ curves scale with temperature in fields around and above B_p . However, the temperature range around 70 K is frequently used to check scaling properties of newly developed materials. The present study shows that the scaling property observed in a narrow temperature window cannot be automatically generalized to a broader temperature range. At temperatures close to T_c , w in both samples shows a fast drop. The parameter n more or less increases from 77 K to 85 K and then drops.

Figure 7(b) shows a stronger temperature dependence of the second peak in comparison to the central peak. For sample LLM the second-peak and central-peak curves cross at around 70 K, irrespective of the experimental method (SQUID and VSM), and above 70 K the central peak becomes dominant. Similarly to w and n , also the magnitudes of the central and second peaks of the MHL, $M_{p1}(T)$ and $M_{p2}(T)$, rapidly drop

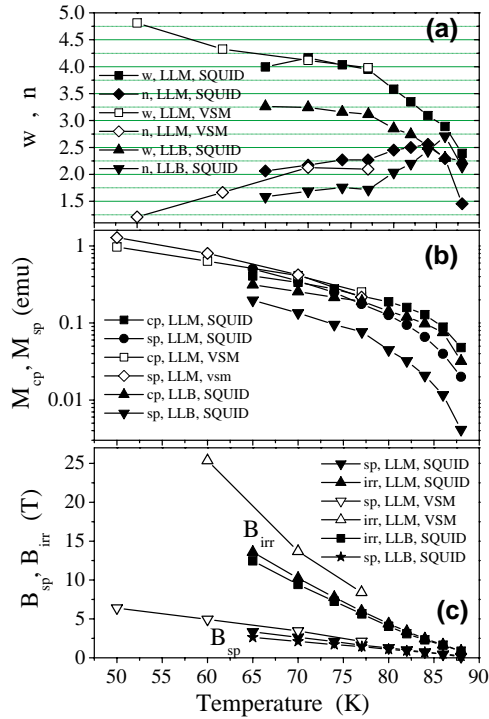


Figure 7. Temperature dependences of (a) the fitting parameters w and n , (b) the magnitudes of the central and second peaks, M_{cp} and M_{sp} , respectively, and (c) the second peak position, B_{sp} and irreversibility field B_{irr} . Both the data inferred from SQUID (full symbols) and VSM experiments (open symbols) are included.

above 85 K. In sample LLB the curves do not cross in the measured temperature range, but the tendency is same as in sample LLM. From this tendency it follows that the curves would cross at about 50 K and only below this temperature would the second peak dominate.

Figure 7(c) shows a nearly linear temperature dependence of the second peak position, B_p for both samples. At low temperatures, a remarkable increase of the B_{irr}/B_p ratio was observed, primarily due to an exceptional increase of B_{irr} . Similar and even stronger increases were also observed in measurements of these samples by VSM at fields up to 15 T⁵.

The fits of the $J_c(B)$ curves measured on sample LLB indicate that even in the case when the second peak is significantly masked by a relatively strong central peak, the $J_c(B)$ curve can be interpreted as a sum of two independent contributions in equation (4). The fit enabled us to separate the two contributions and to study the evolution of the weak second peak as a function of temperature.

From our analysis it follows that there is no principal difference in the magnetic behaviour of these two samples (as well as of the other 10 samples with intermediate properties) and that the second peak always participates in the formation of the MHL shape up to temperatures close to T_c . There is, however, a significant difference of all these melt-textured samples and RE-123 single crystals at low temperatures; for example in sample LLM, the second peak became stronger than the central peak below 70 K. The increase of the ratio J_{p1}/J_{p2} could be observed up to 50 K (VSM experiments). This

⁵ These experiments were performed in the Institute for Material Research, Tohoku University in Sendai, Japan.

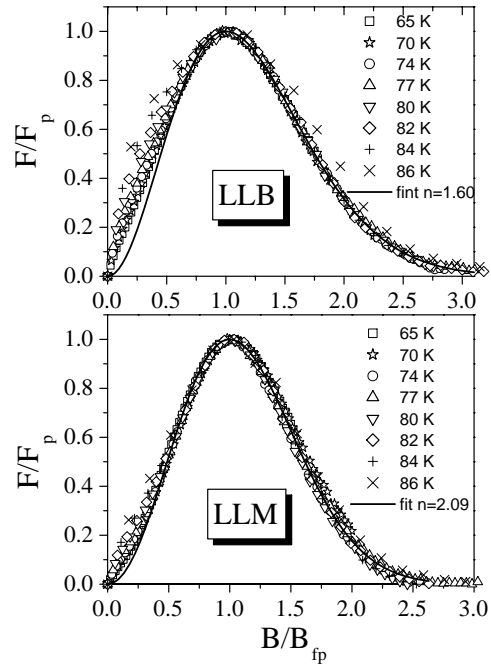


Figure 8. Scaling of pinning force density deduced from the experimental data in figures 5 and 6. The fits indicated by full curves were made by the function $y = x^2 \exp[(1 - x^n)2/n]$, which only takes the second term in equation (4) into account.

means that with decreasing thermal activation the effectiveness of point-like pinning defects increases with respect to the pinning efficiency of secondary-phase particles. Sample LLB developed a similar behaviour.

Another consequence of this effect is that at very low temperatures the second peak in the melt-textured samples has a tendency to mask the central peak, the situation opposite to that in single crystals. In some samples [30] such a situation takes place even at 77 K, which can lead to doubts as to whether the central peak is present in such samples at all. Of course it is present, but it is fully covered by the second peak, which can be verified at higher temperatures.

3.3. Fit of the pinning force density

Figure 7(a) showing the temperature dependence of n , indicates that the scaling of the $J_c(B)$ curves is, in the samples studied, limited to the temperature range 65–77 K. In figure 8 we show the scaling of the pinning force densities deduced from the measured data of samples LLM and LLB as $F = BJ_c$. The $F(B)$ dependence was normalized with respect to the peak coordinates (B_{fp} , $F(B_{fp})$). It is evident that the scaling of $F(B)$ extends over a significantly broader temperature range than that of $J_c(B)$. As $J_c(B)$ and $F(B)$ data representations should be theoretically equivalent, we attribute the different behaviours of these two quantities to the different position of the peak. $F(B)$, as a product of J_c and B , exhibits the peak at significantly higher fields than the corresponding $J_c(B)$. Evidently, the vortex–matter dynamics above B_p is much more uniform than that observed around or below the peak in $J_c(B)$. The suppression of the central peak and the greater distance from the area of the low-field pinning mechanism activity may also play a significant role here. As a result the scaling of $F(B)$

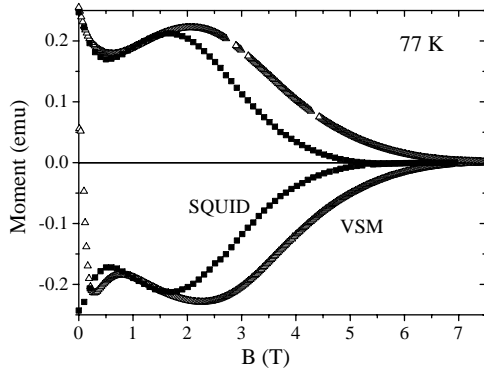


Figure 9. The comparison of the MHLs measured quasistatically by SQUID and dynamically by VSM on the samples and at the same temperature, 77 K. Both curves were corrected for the paramagnetic signal arising from the ND, Eu, and Gd ions. The difference in the irreversibility field is striking. Also, the VSM $M(B)$ curves could be easily modelled by the function (4).

with the applied field normalized to a higher peak field value, B_{fp} , exists in a broader temperature range. This result seems to be quite general, as a good scaling of $F(B)$ has been observed in many other samples. Surprisingly, even in sample LLB with a poorly developed second peak the $F(B)$ scaling was good and the temperature range of this scaling did not differ much from that of sample LLM.

The deviation of the fitting function $y = x^2 \exp[(1 - x^n)/n]$ used for the fit in figure 8 from the experimental data on the low-field slope of the $F(B)$ dependences is caused by the central peak contribution, which does not scale in the manner of the second peak. Although the central peak is, in the $F(B)$ representation, strongly suppressed it manifests itself in this way. This conclusion also follows from the fact that in the LLB sample the ‘non-scaling behaviour’ was stronger than in sample LLM. The reason is simple: in sample LLB the central peak dominated the second peak, while in sample LLM the opposite is true.

3.4. Field sweep effect

The samples LLM and LLB were measured by VSM in fields of up to 14 T (see earlier footnote). This enabled us to extend the temperature range up to 40 K, so that we could still see the second peak maximum within the experimental field range. The field sweep rate was 8.3 mT s^{-1} . A comparison of the quasistatic SQUID measurements and the dynamic VSM measurements is shown in figure 9. Although the magnetic moment did not differ much, there was an enormous difference in B_{irr} , and, consequently, also in B_p . The difference in B_{irr} amounted nearly 3 T at 77 K! This manifests the huge effect of the field sweep and points to the necessity to present any magnetic characterization with a definition of the experimental conditions.

Both the lack of scaling and the rapid growth of B_{irr} at low temperatures imply a rapid change in the pinning energy distribution.

We note that also the VSM data could be easily modelled by the function (4).

4. Conclusions

In the NEG-123 system under study the Gd-211 particles were regularly distributed within the whole pellet. Though the J_{p1} , B_{irr} and B_p were found to be similar in all the samples, the second peak height notably varied from sample to sample. This feature implies a strong effect of local microscopic fluctuations in the 123 matrix properties that cannot be directly related to the secondary-phase particles. These particles might indirectly induce the matrix properties variation (e.g. stacking faults), which would explain the positive effect of the secondary-phase particles refinement on the second peak [11, 12].

All data, with both well developed and suppressed second peaks, could be easily interpreted as a sum of two independent functions of B : a rapidly exponentially decaying low-field one and a high-field exponentially decaying function following from use of the phenomenologically established logarithmic pinning potential modified by a linear increase [19]. This type of fit was fully successful in the entire temperature range, from 50 to 88 K. This procedure enabled us to observe the participation of the separated contributions on the formation of the MHL in a broad temperature range and to estimate B_{irr} even at low temperatures where the irreversibility field was out of the experimental field range. This analysis showed that only the point-like pinning disorder is responsible for the shape of the total magnetization curve at high fields. Only at temperatures close to T_c does the second peak become weak enough so that also the central peak participates in the formation of the MHL high-field tail. The high thermal activation at these temperature eliminates most of the small point-like defects from the pinning process and increases the importance of the larger pinning centres. At the same time the field range is limited so that the specific character of pinning attributed to SPP (we believe it is surface pinning) can take place. This all is consistent with the experimental evidence of the effect of SPP on the central peak [11, 12].

The extended temperature range of the scaling observed in the $F(B)$ dependence with respect to that of $J_c(B)$ gave evidence of much more uniform flux dynamics at fields above B_p than below or around it.

Although the role of the second peak decreases with increasing temperature, it is present, at least in the weak form, up to temperatures close to T_c . On the other hand, with decreasing temperature, the second peak becomes dominant and can eventually completely mask the central peak; but even in the case that the central peak is fully masked by the huge second peak, the pinning mechanism standing behind the central peak still contributes to the shape of the total magnetization curve.

The VSM measurements showed a strong effect of the field sweep rate, especially on B_{irr} , which points to difficulties in comparing data obtained by different experimental methods and implies the necessity to standardize the conditions for magnetic characterization of new materials.

Acknowledgments

M Jirsa greatly appreciates the JSPS fellowship covering his working stay at Iwate University, Morioka, Japan, and the

partial support by the grant No A1010919/99 of the Grant Agency of the ASCR. M Muralidhar acknowledges the support from a NEDO fellowship.

References

- [1] Zhukov A A, Küpfer H, Perkins G, Cohen L F, Caplin A D, Klestov S A, Claus H, Voronkova V I, Wolf Th and Wühl H 1995 *Phys. Rev. B* **51** 12 704
- [2] Jirsa M, Koblishka M R, Higuchi T and Murakami M 1998 *Phys. Rev. B* **58** R14 771
- [3] Erb A, Genoud J-Y, Marti F, Däumling M, Walker E and Flükiger R 1996 *J. Low Temp. Phys.* **105** 1023
- [4] Küpfer H, Wolf Th, Lessing C, Zhukov A A, Lançon X, Meier-Hirmer R, Schauer W and Wühl H 1998 *Phys. Rev. B* **58** 2886
- [5] Egi T, Kuroda K, Unoki H and Koshizuka N 1995 *Appl. Phys. Lett.* **67** 2406
- [6] Chikumoto N, Yoshioka J and Murakami M 1997 *Physica C* **291** 79
- [7] Freyhardt H C 1971 *Phil. Mag.* **23** 369
- [8] Dew-Hughes D 1974 *Phil. Mag.* **30** 293
- [9] Blackstead H A and Dow J D 1997 *Appl. Phys. Lett.* **70** 1891
- [10] Iwata S, Nagaya S, Ikuta H and Mizutani U 1998 *Advances in Superconductivity* vol X, ed K Osamura and I Hirabayashi (Tokyo: Springer) p 657
- [11] Muralidhar M, Koblishka M R, Saitoh T and Murakami M 1998 *Supercond. Sci. Technol.* **11** 1349
- [12] Muralidhar M, Koblishka M R and Murakami M 1999 *Eur. Phys. J.* **7** 99
- [13] Muralidhar M, Koblishka M R, Diko P and Murakami M 2000 *Appl. Phys. Lett.* **76** 91
- [14] Wang Z L, Goyal A and Kroeger D M 1993 *Phys. Rev. B* **47** 5373
- [15] Harada K, Kasai H, Kamimura O, Matsuda T, Yoshida T, Tonomura A, Shimoyama J, Kishio K and Kitazawa K 2000 *Advances in Superconductivity* vol XII, ed J Tamashita and K Tanabe (Tokyo: Springer) p 287
- [16] Perkins G K, Cohen L F, Zhukov A A and Caplin A D 1995 *Phys. Rev. B* **51** 8513
- [17] Perkins G K and Caplin A D 1996 *Phys. Rev. B* **54** 12 551
- [18] Jirsa M, Püst L, Dlouhý D and Koblishka M R 1997 *Phys. Rev. B* **55** 3276
- [19] Jirsa M, Koblishka M R, Muralidhar M, Higuchi T and Murakami M 2000 *Physica C* **338** 235
- [20] Jirsa M and Püst L 1997 *Physica C* **291** 17
- [21] Senoussi S, Ouasséna M, Collin G and Campbell I A 1988 *Phys. Rev. B* **37** 9792
- [22] Kimura T, Kishio K, Kobayashi T, Nakayama Y, Motohira N, Kitazawa K and Yamafuji K 1992 *Physica C* **192** 247
- [23] Kobayashi T, Kimura T, Shimoyama J, Kishio K, Kitazawa K and Yamafuji K 1995 *Physica C* **254** 213
- [24] Mochida T, Chikumoto N and Murakami M to be published
- [25] Koblishka M R, Muralidhar M and Murakami M 2000 *Advances in Superconductivity* vol XII, ed J Tamashita and K Tanabe (Tokyo: Springer) p 359
- [26] Murakami M 1992 *Melt Processes High Temperature Superconductors* (Singapore: World Scientific)
- [27] Däumling M and Larbalestier D C 1989 *Phys. Rev. B* **40** 9350
- [28] Däumling M, Walker E and Flükiger R 1994 *Phys. Rev. B* **50** 1302
- [29] Däumling M, Walker E, Grasso G and Flükiger R 1994 *ICMC Topical Conf. on Critical State in Superconductors (Honolulu, HI, October 1994)*
- [30] Muralidhar M and Murakami M 2000 *Supercond. Sci. Technol.* **13** 1315